PCCP

PAPER

View Article Online
View Journal

Cite this: DOI: 10.1039/d5cp02842f

Low-energy modes and localized excitations in metal halide perovskites: insights from heat capacity

Ana Arauzo, *[a] Pelayo Marin-Villa, [b] Kacper Drużbicki, [c] María Concepción Sánchez [d] and Felix Fernandez-Alonso *[bef]

Received 25th July 2025,
Accepted 8th September 2025

DOI: 10.1039/d5cp02842f

rsc.li/pccp

Metal halide perovskites (MHPs) hold great potential to integrate future mass-produced photovoltaic technologies owing to their exceptional power conversion efficiencies and charge-carrier transport properties. However, their performance is still hindered by a poor understanding of their complex soft structures and the role played by defects and impurities in their optoelectronic properties. For the first time, the molar heat capacities of two archetypal MHPs – $MAPbI_3$ and $FAPbI_3$ – as well as two thermodynamically stable non-perovskite specimens δ-$FAPbI_3$ and δ-$CsPbI_3$ have been measured down to 0.35 K. The behavior of the four crystals below 10 K departs notably from the predictions of the Debye model. All samples exhibit a broad feature in the Debye-reduced C/T^3 representation that can be interpreted from harmonic lattice dynamics calculations as the excitation of low-energy optical vibrations. We also find that in all cases, the sub-Kelvin regime evinces a common trend across all samples, which may be interpreted within the framework of incoherent tunneling. The application of a magnetic field enables microscopic assessment of two-level systems in δ-$FAPbI_3$, identifying them as intrinsic paramagnetic centers. These findings highlight the universal presence of low-energy excitations in MHPs and their crucial link to dynamic disorder, providing a deeper understanding of the microscopic origins of phase instability and thermal anomalies in this class of materials.

Introduction

Metal halide perovskites (MHPs) are regarded as promising candidates for a new generation of cheaper and more sustainable photovoltaics and light-emitters.[1–4] Notwithstanding the success they enjoy to date owing to a sharp rise in power conversion efficiency of MHP-based devices,[5–8] a series of challenges continue to prevent MHPs from becoming a thriving class of materials in the energy sector. Undesired phase transitions, structural degradation due to the exposure to moisture and UV radiation severely affect the aforementioned properties by driving the fragile perovskite framework into decomposition.[9,10] Thus, unraveling the rationale behind phase stabilization is mandatory to enhance future developments, including extending the (thermal) operational range of MHP-based devices.[11,12]

The polymorphism exhibited by MHPs is rooted in several factors. One of them is the presence of weakly bonded, heavy metallic and halide atoms forming characteristic octahedral networks. This situation leads to low-energy vibrational modes and intrinsic dynamic disorder even at temperatures close to zero.[13–16] Caesium lead iodide, $CsPbI_3$, crystallizes in a yellow, non-perovskite orthorhombic structure (δ-$CsPbI_3$, *Pnma* space group). Nonetheless, it is possible to drive the system to a black, perovskite cubic phase (α-$CsPbI_3$, $Pm\bar{3}m$ space group) by heating above 583 K.[17,18] The perovskite framework is retained in two subsequent phase transitions to the tetragonal β-$CsPbI_3$ (*P4/mbm* space group) and the orthorhombic γ-$CsPbI_3$ (*Pbnm* space group) structures at 510 and 325 K, respectively.[19] We underline that although both δ and γ phases share the orthorhombic symmetry, their atomic frameworks exhibit strong differences. For instance, while the γ-$CsPbI_3$ phase adopts the characteristic corner-shared network of PbI6- octahedra found in three-dimensional perovskites, the δ-$CsPbI_3$ structure features 1D chains of face-sharing PbI6- octahedra. Thus,

[a] Instituto de Nanociencia y Materiales de Aragón (INMA), CSIC-Universidad de Zaragoza, and Departamento de Física de la Materia Condensada, 50009 Zaragoza, Spain. E-mail: aarauzo@unizar.es
[b] Centro de Física de Materiales (CFM-MPC), CSIC-UPV/EHU, Paseo de Manuel Lardizabal 5, Donostia, 20018, Gipuzkoa, Spain. E-mail: felix.fernandez@ehu.eus
[c] Polish Academy of Sciences, Centre of Molecular and Macromolecular Studies, Sienkiewicza 112, 90-363 Lodz, Poland
[d] Instituto de Nanociencia y Materiales de Aragón (INMA), CSIC-Universidad de Zaragoza, Pedro Cerbuna 12, 50009 Zaragoza, Spain
[e] Donostia International Physics Center (DIPC), Paseo de Manuel Lardizabal, 4, 20018 Donostia - San Sebastian, Spain
[f] IKERBASQUE, Basque Foundation for Science, Plaza Euskadi, 5, 48009 Bilbao, Spain

octahedral connectivity is the key structural factor differentiating the γ-phase. The above phases can be identified using X-ray diffraction – see Fig. S2.

In MHPs with an organic cation, chemical moieties add extra degrees of freedom, charge anisotropy, and interactions such as hydrogen bonds. Cation motions and their associated orientational entropies contribute decisively to stabilizing the structures.[20,21] Such is the case for methylammonium lead iodide, $MAPbI_3$, and its formamidinium analogue, $FAPbI_3$. The first one has three perovskite phases at ambient pressure: a cubic phase (α) above 330 K, a tetragonal phase (β) between 330 and 160 K, and a orthorhombic phase (γ) below 160 K.[22] The relationship between the different phases of $FAPbI_3$ is more complex and, still, less understood. Similarly to the caesium case, $FAPbI_3$ adopts a yellow, non-perovskite phase at ambient conditions (δ-$FAPbI_3$). The crystal structure of δ-$FAPbI_3$ follows a hexagonal pattern that falls under the $P6_3/mmc$ space group. This phase later transforms to a low-temperature hexagonal phase ($P6_3/m$) below 175 K.[23] Nonetheless, it is possible to reach a black, cubic perovskite phase (α-$FAPbI_3$, $Pm\bar{3}m$) at high temperatures followed by a cascade of transformations: one continuous transition from cubic to tetragonal (β-$FAPbI_3$) at 280 K, another isostructural tetragonal-tetragonal through an intermediate state at 140 K, and a final orthorhombic (γ-$FAPbI_3$) phase.[24,25] The latter case conforms to an orientational glass, underscoring the distinct dynamic behavior of the FA^+ cation and the challenging determination of structural models for this material.[26,27]

In the above context, it is clear that a multi-technique approach beyond standard Bragg diffraction is mandatory in order to rationalize the complex dynamics and the underlying atomic structures of MHPs. In particular, the analysis of thermophysical data has already provided solid grounds for scrutinizing the behavior of MHPs.[28–30] Since the (molar) heat capacity depends directly on the vibrational density of states (VDoS), it can validate proposed structural models *via* lattice dynamics calculations.[30] This procedure has revealed the mechanical origin of the "boson peak" in crystalline systems.[31] Phenomenological theories like the standard tunneling model (STM)[32,33] and the soft potential model (SPM)[34,35] have been developed to provide a quantitative appraisal of heat capacity data where the use of mechanical models to explain thermophysical data becomes problematic, *e.g.*, glasses or where non-acoustic phonon contributions are increasingly suppressed. Both postulate the that some atoms or groups of atoms tunnel between nearly equivalent configurations, resulting in two-level systems (TLS) which give rise to a linear temperature dependence of the heat capacity – $C \propto T$.[32,33] None of the abovementioned theories, however, provide any indication regarding the physical origin of their contributions. The lack of a microscopic description leaves the door open to a wide range of possible sources of TLS contributing to the sub-Kelvin heat capacity. Ultimately, it seems reasonable that the nature of tunneling systems depends on the atomic or molecular landscape of the crystal. Crystal imperfections (vacancies, interstitials, off-center atoms) create atomic-level distortions where atoms or molecules tunnel between nearly degenerate states and generate strain in the lattice, affecting the optoelectronic properties.[36,37] Among these, iodine interstitials, are known to bond to one lattice iodine and form I_2^- dimers. These are called H-centers by the MHP community and have a characteristic paramagnetic $S = \frac{1}{2}$ spin configuration.[37] Their identification and control remain a major challenge in the field.[38] Applying an external magnetic field could reveal the presence of these centers by lifting the degeneracy of the different spin states.

Building upon the above, we report a comprehensive study on the heat capacity of four MHP samples ($MAPbI_3$, $FAPbI_3$, δ-$FAPbI_3$ and δ-$CsPbI_3$). Our findings evince that the temperature dependence of the heat capacity at cryogenic temperatures deviates from the predictions given by the (sole) contribution of acoustic modes for all samples. These departures from expectation manifest themselves in various ways. The first one is the appearance of a broad feature in the Debye-reduced C/T^3 representation near 6 K. In line with our previous work,[30] harmonic lattice dynamics (HLD) calculations using on available structural models – see Fig. S1 – provide a mechanical interpretation for δ-$CsPbI_3$ based on the excitation of low-energy optical vibrations. In the sub-Kelvin regime, we find a power-law behavior common to all samples that is consistent with a random distribution of TLS similar to those found in non-metallic glasses.[39,40] These measurements reveal a heat capacity excess of nearly two orders of magnitude in the case of δ-$FAPbI_3$ relative to the other samples, and in particular to the $FAPbI_3$ perovskite. This finding motivates a quantitative assessment of the number of paramagnetic centers arising from point defects in δ-$FAPbI_3$.

Heat capacity predictions using HLD

Fig. 1 and Fig. S3 show the the temperature dependence of experimental molar heat capacity recorded for $MAPbI_3$, $FAPbI_3$, δ-$FAPbI_3$ and δ-$CsPbI_3$. The data were further normalized to the

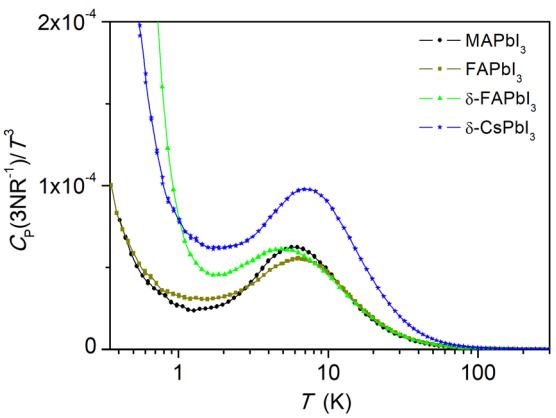

Fig. 1 Debye-reduced heat capacity C_P/T^3 as a function of temperature. $MAPbI_3$ (black circles), $FAPbI_3$ (dark-green squares), δ-$FAPbI_3$ (light green triangles) and δ-$CsPbI_3$ (blue stars). Color lines are guides to the eye.

classical limit of $3NR$, where N is the number of atoms per formula-unit and R is the universal gas constant. The Debye-reduced C_P/T^3 representation in Fig. 1 underlines the departure from the sole contribution of acoustic modes to the heat capacity.[41] This behavior yields a pronounced feature centered between 5 and 7 K, depending on the sample – in particular, 5.9 K for $MAPbI_3$, 6.3 K for $FAPbI_3$, 5.0 for δ-$FAPbI_3$ and 7.1 K for δ-$CsPbI_3$. Similar (broad) characteristic features have been observed in many disordered or glassy systems,[31] and was previously reported for $FAPbI_3$ and $MAPbI_3$.[25,28] In the latter case, a mechanical explanation based on the excitation of sub-THz (1.5–4.5 meV) vibrational modes was supported by HLD calculations of its low-temperature structure.[30] For $FAPbI_3$, the lack of sound structural models of its low-temperature phase owing to its glassy nature hinders the use of a similar protocol to scrutinize the origin of the thermophysical deviations.[26,27,42]

In the light of the above, we focused on modeling the vibrational response of the inorganic analogue using three available crystallographic structures extracted from ref. 19 and 43 – see models together with their calculated phonon dispersions in Fig. S1. The non-perovskite orthorhombic (*Pnma*) model is taken from a crystallographic analysis by Straus *et al.*[43] Two alternative, and virtually identical, structural models for the perovskite low-temperature phase are also considered: a *Pnma* one also proposed by Straus *et al.*, and a *Pnam* structure reported by Marronnier *et al.*[19] These two models of the γ phase models differ slightly in their symmetry settings and octahedral tilt systems, resulting in nearly indistinguishable diffraction patterns and very similar structural frameworks. The selection of the PBEsol[44] approximation to the exchange–correlation energy in our first-principles calculations was motivated by our previous works on the vibrational properties of HPs,[30,45,46] – details of the calculations can be found in Section S1. HLD calculations grant us with access to the dispersion relations, *i.e.*, the harmonic energy $E_{\mathbf{k}j}$ of a given mode j for a wave-vector $\mathbf{k}$ for the set of $CsPbI_3$ models. Close inspection of the results in Fig. S1 reveals that although both perovskite structures, *Pnma* and *Pnam*, have extremely low-energy (vibrational) modes in the first Brillouin zone, all three structures remain mechanically stable. Therefore, the isochoric heat capacity can be computed according to the following relation

$$C = \sum_{k,j} \frac{\exp\left(\frac{E_{\mathbf{k}j}}{k_B T}\right)}{\left(\frac{E_{\mathbf{k}j}}{k_B T} - 1\right)^2} \left(\frac{E_{\mathbf{k}j}}{k_B T}\right)^2. \quad (1)$$

These results were further normalized to the thermodynamic limit of $3NR$ for direct comparison against experimental data. Fig. 2 confirms that calculations of the δ-$CsPbI_3$ model describe qualitatively the divergence from the canonical solid behavior down to *ca.* 2 K. On the other hand, the predicted heat capacities for the two perovskite models manifest a upsurge between 2 and 10 K reminiscent of the substantial softening of both acoustic and optical branches below the half-meV mark

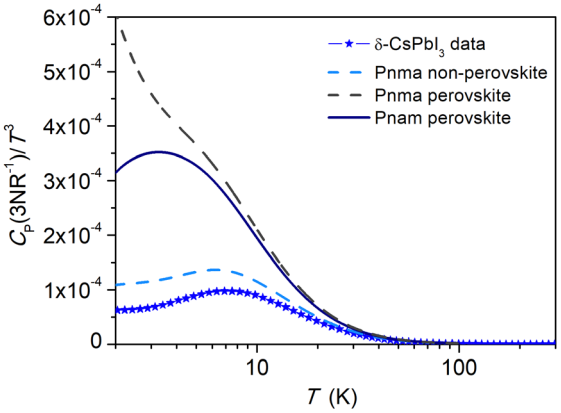

Fig. 2 Experimental (blue stars) and theoretical (blue lines) $C_P(T)/T^3$ obtained for three structural models of $CsPbI_3$.

seen in Fig. S1. Our findings reveal that dispersion relations in this material are very sensitive to the choice of Density Functional Approximation (DFA). Indeed, the *meta*-GGA SCAN functional suppresses the Γ-point instabilities previously reported using LDA, which were indicative of ferroelectric behavior.[47] Similarly, no such instabilities are observed at the PBEsol level for the structures examined in this work.

Heat capacities in the sub-Kelvin regime

At this point, we turn our attention to the hardly explored regime of sub-Kelvin temperatures. In this low-temperature limit, the available thermal energy is of the order of μeV, resulting in negligible excitation of collective lattice vibrations. Consequently, the conventional phonon picture derived from HLD calculations fails to account for a significant portion of the observed thermophysical properties in this regime. The data displayed in Fig. 1 and Fig. S3 indicates that they follow different trends below the maximum of the Debye-reduced shoulder. In the case of the perovskite structures, $MAPbI_3$ and $FAPbI_3$, both exhibit an almost identical, monotonically decreasing trend with temperature. On the contrary, the non-perovskite analogue δ-$FAPbI_3$ Exhibits a noticeable upturn beginning at 1 K, driving the heat capacity to values nearly two orders of magnitude higher than those of the perovskite phases. Moreover, δ-$CsPbI_3$ lies effectively in the middle between the previous trends. These measurements are consistent with previous reports in the literature down to 1 K.[29,48]

While this temperature regime remains unexplored for MHPs, there are examples of earlier reports which accessed it for a breadth of glasses and minimally disordered crystals alike.[40,49] The STM is used readily to explain the linear dependence with temperature according to random distributions of TLS arising from the configurational disorder. Although the purported universality of this behavior for glasses has been put into question,[49] it is nonetheless striking that a linear scaling of the heat capacity with temperature holds for materials whose

microscopic structure and dynamics are remarkably different. Alternatively, the SPM is an extension of the former model which incorporates a broad distribution of asymmetric anharmonic potentials governing atomic or molecular displacements.[34,35] Based on this, we decided to explore the universality of the power law for all measured specimens using an extension of another theory, *i.e.*, the SPM, which includes additional contributions like Debye's and additional anharmonic low-energy modes. The results of these fits are shown in Fig. S5 and Table S1. Although the SPM provides a sensible explanation of the experimental data down to the lowest measured temperatures for both perovskite samples, it misses the upturn experienced by δ-$FAPbI_3$ and δ-$CsPbI_3$ below *ca.* 1.5 K. In order to address the diverging trends, we performed an alternative analysis of the heat capacity data below the maximum in the Debye-reduced plot. In this case, the SPM was extended by allowing the first term to vary freely during the optimization process. Thus:

$$C_P/T^3 = C_{LT}T^{\alpha} + C_D + C_{SM}T^2, \quad (2)$$

where C_{LT} is the low temperature linear term, α is the power exponent allowed to vary freely, C_D is the Debye coefficient, and C_{SM} is a fifth power coefficient accounting for the low-energy modes contribution. The inclusion of a power-law term T^{α} substantially improves the fit over the $\alpha = -2$ for both δ-$CsPbI_3$ and δ-$FAPbI_3$, where the divergent contribution is more pronounced – see Fig. 3a for the corresponding fits using eqn (2). A particularly good agreement is achieved for the non-perovskite samples, while C_{LT} carries a relatively large uncertainty for $MAPbI_3$ and $FAPbI_3$. To better illustrate the power law at low temperatures, Fig. 3b displays the temperature evolution of the α exponent, obtained from the logarithmic derivative of $\log(C_P/T^3)$ with respect to $\log(T)$. All fitted exponents exhibit a common trend towards $\alpha = -2$ at the lowest measured temperatures, within three standard deviations. This universal behavior suggests that the heat capacity in MHPs at very low temperatures originates from a distribution of TLS, consistent with the standard tunneling model (STM).

Paramagnetic behavior of δ-$FAPbI_3$

Our thermophysical measurements reveal a disparity of nearly two orders of magnitude between the perovskite and non-perovskite forms of $FAPbI_3$, as displayed in Fig. S6. Given that the non-perovskite phase was obtained by thermal annealing of its hexagonal precursor, the observed excess heat capacity must originate from an intrinsic feature of the non-perovskite lattice structure. We note that the absence of reliable structural data on γ-$FAPbI_3$ prevents us from comparing the perovskite and non-perovskite structures to draw a structural origin of the TLS. Moreover, the low-temperature behavior is dominated by a broad distribution of TLS, consistent with the characteristic heat-capacity response depicted in Fig. 3. One possibility is that defects, particularly H-centers, produce Schottky-like contributions to the heat capacity due to their paramagnetic spin configuration $S = \frac{1}{2}$.[50] Such contributions to the heat capacity obey the following relation:

$$C = k_B\left(\frac{\Delta E}{k_B T}\right)^2 \frac{e^{\frac{\Delta E}{k_B T}}}{\left(1 + e^{\frac{\Delta E}{k_B T}}\right)^2}, \quad (3)$$

where ΔE denotes the energy splitting of the two spin states under an effective magnetic field H_{eff} such that $\Delta E = g\mu_B H_{eff}$ (with $g \approx 2$ and μ_B the Bohr magneton).

To investigate the magnetic nature of the observed thermal anomaly, we conducted heat capacity measurements under applied magnetic fields ranging from 1 T to 14 T. The data, presented in the Debye-reduced form C_P/T^3 in Fig. 4a, exhibit a logarithmic suppression of heat capacity at sub-Kelvin temperatures with increasing magnetic field. Specifically, at 14 T, the heat capacity is reduced by nearly a factor of three compared to the zero-field measurement, thereby reinforcing the magnetic origin of the observed feature.

Fig. 4b shows that these results are compatible with an estimated concentration of 0.8% H-centers per mole of

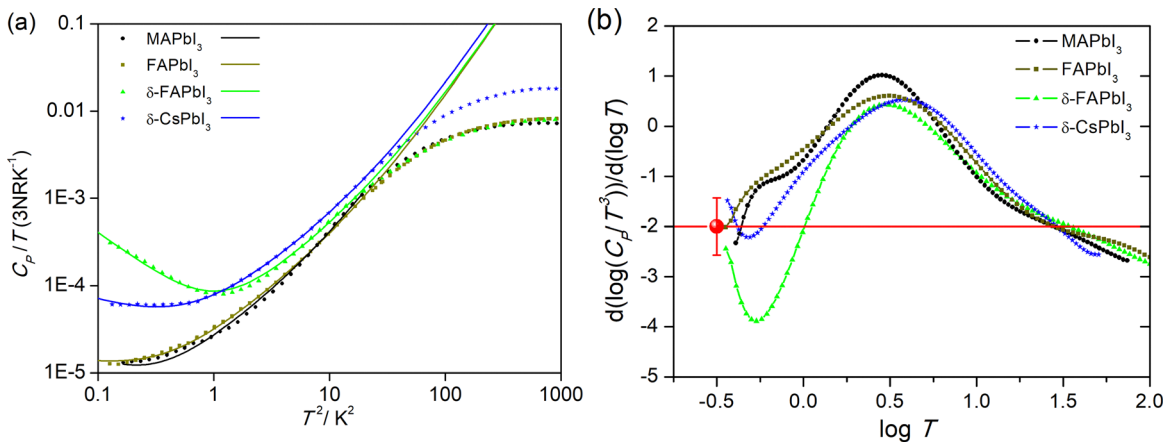

Fig. 3 (a) Temperature squared dependence of C_P/T. Lines are the fits to eqn (2), fit parameters are given in Table 1. (b) Temperature dependence of alpha exponent α obtained from the derivative of $\log(C_P/T^3)$ with respect to $\log(T)$ plotted as a function of $\log(T)$. The red dot is the mean value at 0.35 K, with a 3-sigma error bar, centered at the STM limit where $\alpha = -2$.

Table 1 Results of the fits below 4 K for the following model: $C_P/T = C_{LT}T^{\alpha+2} + C_D T^2 + C_{SM}T^4$

	C_{LT} (mJ mol^{-1} K^{-2})	α	C_D (mJ mol^{-1} K^{-4})	C_{SM} (mJ mol^{-1} K^{-6})
$MAPbI_3$	0.6 ± 0.3	−3 ± 1	6.9 ± 0.3	0.57 ± 0.03
$FAPbI_3$	1.8 ± 0.3	−2.4 ± 0.4	5.7 ± 0.3	0.66 ± 0.03
δ-$FAPbI_3$	13.5 ± 0.6	−3.9 ± 0.1	12.0 ± 0.3	0.39 ± 0.03
δ-$CsPbI_3$	3.1 ± 0.1	−2.8 ± 0.1	6.5 ± 0.1	0.20 ± 0.01

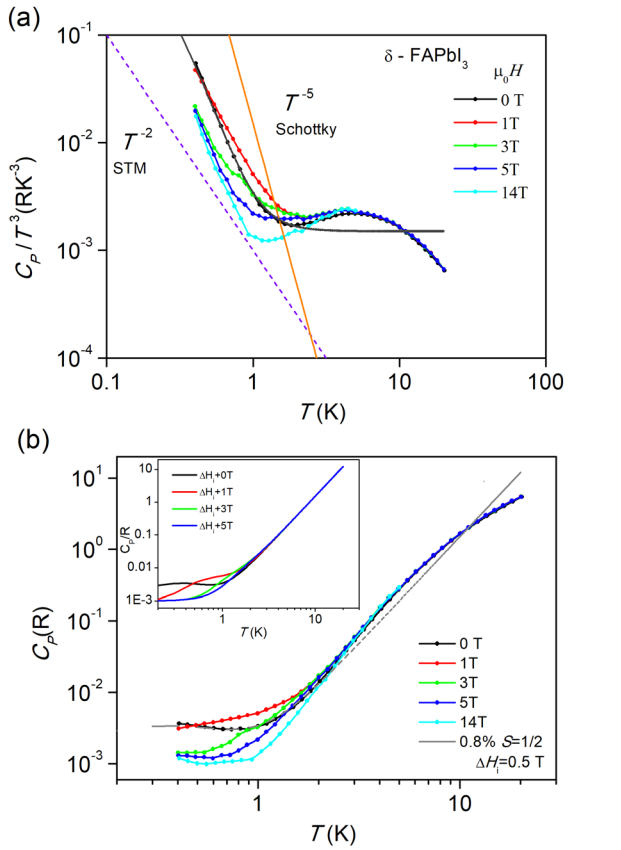

Fig. 4 (a) Debye-reduced specific heat of δ-$FAPbI_3$ as a function of temperature and magnetic field. The lines labelled T^{-2} and T^{-5} represent power-law behaviours corresponding to the STM and the high T limit of a Schottky anomaly respectively. (b) Heat capacity $C_P(T,H)$. The grey line is the estimated magnetic contribution arising from a concentration of 0.8% S = 1/2 magnetic impurities, experiencing internal magnetic fields distributed uniformly between 0 and 1 T. Inset illustrates the simulation of C_P for this distribution of spin centers under the same external magnetic fields.

δ-$FAPbI_3$, accompanied by an energy distribution width of approximately 0.1 meV. This spread is consistent with the internal strain present in the non-perovskite phase, likely originating from local distortions and disorder. Dipolar and hyperfine interactions involving iodine nuclei ($I = \frac{5}{2}$ for 100% ^{127}I) can lift the degeneracy of the spin states and further modulate the TLS landscape. Interestingly, increasing the applied magnetic field shifts the TLS contribution from 1.34 K at 1T to approximately 15 K at 14 T, consistent with Zeeman energy scaling. This shifting peak evidences the sensitivity of these centers to external perturbations and supports a scenario where both disorder and internal strain together lead to the excess heat capacity. These results are also consistent with the reduction of lattice strain after annealing, since the perovskite structure does not show this energetic surplus. Furthermore, the presence of a residual, non-magnetic heat capacity component, persisting even at 14 T, indicates the contribution of alternative mechanisms. Among them, transitions between rotational states of the FA^+ cations are a plausible source.[51]

Conclusions

This work presents a detailed investigation of the heat capacity of four MHPs – $MAPbI_3$, $FAPbI_3$, δ-$FAPbI_3$, and δ-$CsPbI_3$ – extending down to the sub-Kelvin temperature regime, in order to elucidate the vibrational and defect-related contributions responsible for deviations from canonical crystalline behavior. Across all samples, heat capacity data display marked departures from the expected Debye law. Notably, a broad excess in the Debye-reduced representation C_P/T^3 near 6 K indicates the presence of low-energy excitations. HLD calculations for δ-$CsPbI_3$ attribute this feature to low-energy optical phonons in mechanically stable perovskite structures. In the sub-Kelvin regime, where phononic contributions become negligible, our analysis suggests a universal trend characterized by a linear term reminiscent of TLS. These behaviors are effectively captured by a modified SPM incorporating a variable power-law term. Particularly, δ-$FAPbI_3$ and δ-$CsPbI_3$ exhibit significant upturns below 1.5 K, indicating a dominant contribution from low-energy excitations associated with structural disorder or point defects. These results demonstrate that crystalline imperfections play an important role in defining the thermophysics of MHPs at cryogenic temperatures. Taken together, our findings underscore that careful examination of heat capacity data across multiple temperatures provides a valuable route to address open structural issues concerning MHPs. This study paves the way for defect-sensitive thermodynamic analyses to monitor H-centers in MHPs. We anticipate that more structural information related to the low-temperature phases of MHPs is mandatory to draw a sharper picture of the structural defects.

Materials and methods

Thermophysical experiments were carried out using samples with a purity exceeding 99% from Xi'an Polymer Light Technologies. The black perovskite (α) phase of $FAPbI_3$ was obtained from the initial yellow (δ) powder by annealing for 4 hours at 150 °C under high vacuum (6 × 10^{-5} mbar) using a two-stage rotary pump. The sample was placed in a quartz tube furnace, with the temperature ramped up at a rate of 3 K min^{-1}, held constant for 4 hours, and then cooled down to room temperature at 6 K min^{-1}. Following this thermal treatment, the

powder turned dark grey to black and remained in the metastable perovskite phase for over a month.

The integrity of the samples, and the presence of both perovskite and non-perovskite phases was confirmed using powder X-ray diffraction (PXRD) – see Fig. S2.

Conflicts of interest

There are no conflicts of interest to declare.

Data availability

Further data supporting this article have been included as part of the SI. Section S1 Computational details. Section S2 Additional experimental details: S2.1, Powder X-ray diffraction; S2.2, Molar heat capacities; S2.3, Debye temperatures; S2.4, Low temperature calorimetric fits; and S2.5, Entropies. See DOI: https://doi.org/10.1039/d5cp02842f.

Additional data that support the findings of this study are available from the corresponding authors upon request.

Acknowledgements

Financial support for this work has been secured through Grants PID2020-114506GB-I00 (funded by MCIN/AEI/10.13039/501100011033); TED2021-129457B-I00 (funded by MCIN/AEI/10.13039/501100011033 and the European Union NextGenerationEU/PRTR); PID2023-146442NB-I00 (funded by MCIU); and PRE2021-097712 (funded by MCIN/AEI/10.13039/501100011033 and by the European Social Fund Programme 'Investing in Your Future'). We acknowledge Poland's PLGrid (Grant PLG/2024/plghybrids2024), the Spanish Supercomputing Network (RES Activity QHS-2023-1-0027), the DIPC Supercomputing Center (Atlas Facility), and UK Research & Innovation (SCARF-RAL Cluster) for access to high-performance-computing resources. We gratefully acknowledge the continued financial support received from the IKUR Strategy under the collaboration agreement between Ikerbasque Foundation and the Materials Physics Center, on behalf of the Department of Science, Universities & Innovation of the Basque Government. Authors would like to acknowledge the use of Servicio General de Apoyo a la Investigación-SAI, Universidad de Zaragoza.

References

1 V. Gonzalez-Pedro, E. J. Juarez-Perez, W.-S. Arsyad, E. M. Barea, F. Fabregat-Santiago, I. Mora-Sero and J. Bisquert, General Working Principles of $CH_3NH_3PbX_3$ Perovskite Solar Cells, *Nano Lett.*, 2014, **14**, 888–893.

2 N. J. Jeon, J. H. Noh, W. S. Yang, Y. C. Kim, S. Ryu, J. Seo and S. I. Seok, Compositional engineering of perovskite materials for high-performance solar cells, *Nature*, 2015, **517**, 476–480.

3 M. (Mariska) de Wild-Scholten, Energy payback time and carbon footprint of commercial photovoltaic systems, *Sol. Energy Mater. Sol. Cells*, 2013, **119**, 296–305.

4 X. Tian, S. D. Stranks and F. You, Life cycle energy use and environmental implications of high-performance perovskite tandem solar cells, *Sci. Adv.*, 2020, **6**, eabb0055.

5 K. Lin, *et al.*, Perovskite light-emitting diodes with external quantum efficiency exceeding 20 per cent, *Nature*, 2018, **562**, 245–248.

6 J. C. Yu, D. B. Kim, E. D. Jung, B. R. Lee and M. H. Song, High-performance perovskite light-emitting diodes via morphological control of perovskite films, *Nanoscale*, 2016, **8**, 7036–7042.

7 Z.-K. Tan, R. S. Moghaddam, M. L. Lai, P. Docampo, R. Higler, F. Deschler, M. Price, A. Sadhanala, L. M. Pazos, D. Credgington, F. Hanusch, T. Bein, H. J. Snaith and R. H. Friend, Bright light-emitting diodes based on organometal halide perovskite, *Nat. Nanotechnol.*, 2014, **9**, 687–692.

8 G. Xing, N. Mathews, S. S. Lim, N. Yantara, X. Liu, D. Sabba, M. Grätzel, S. Mhaisalkar and T. C. Sum, Low-temperature solution-processed wavelength-tunable perovskites for lasing, *Nat. Mater.*, 2014, **13**, 476–480.

9 L. Meng, J. You and Y. Yang, Addressing the Stability Issue of Perovskite Solar Cells for Commercial Applications, *Nat. Commun.*, 2018, **9**, 5265–5274.

10 I. Deretzis, E. Smecca, G. Mannino, A. L. Magna, T. Miyasaka and A. Alberti, Stability and Degradation in Hybrid Perovskites: Is the Glass Half-Empty or Half-Full?, *J. Phys. Chem. Lett.*, 2018, **9**, 3000–3007.

11 Y. Xu, Z. Wu, Z. Zhang, X. Li and H. Lin, Evolved photovoltaic performance of $MAPbI_3$ and $FAPbI_3$-based perovskite solar cells in low-temperatures, *Energy Mater.*, 2024, **4**, 400034.

12 E. M. Mozur and J. R. Neilson, Cation Dynamics in Hybrid Halide Perovskites, *Annu. Rev. Mater. Sci.*, 2021, **51**, 269–291.

13 T. Lanigan-Atkins, X. He, M. J. Krogstad, D. M. Pajerowski, D. L. Abernathy, G. N. M. N. Xu, Z. Xu, D.-Y. Chung, M. G. Kanatzidis, S. Rosenkranz, R. Osborn and O. Delaire, Two-dimensional overdamped fluctuations of the soft perovskite lattice in $CsPbBr_3$, *Nat. Mater.*, 2021, **20**, 977–983.

14 O. Yaffe, Y. Guo, L. Z. Tan, D. A. Egger, T. Hull, C. C. Stoumpos, F. Zheng, T. F. Heinz, L. Kronik, M. G. Kanatzidis, J. S. Owen, A. M. Rappe, M. A. Pimenta and L. E. Brus, Local Polar Fluctuations in Lead Halide Perovskite Crystals, *Phys. Rev. Lett.*, 2017, **118**, 136001.

15 M. J. Schilcher, P. J. Robinson, D. J. Abramovitch, L. Z. Tan, A. M. Rappe, D. R. Reichman and D. A. Egger, The Significance of Polarons and Dynamic Disorder in Halide Perovskites, *ACS Energy Lett.*, 2021, **6**, 2162–2173.

16 O. Cannelli, J. Wiktor, N. Colonna, L. Leroy, M. Puppin, C. Bacellar, I. Sadykov, F. Krieg, G. Smolentsev, M. V. Kovalenko, A. Pasquarello, M. Chergui and G. F. Mancini, Atomic-Level Description of Thermal Fluctuations in Inorganic Lead Halide Perovskites, *J. Phys. Chem. Lett.*, 2022, **13**, 3382–3391.

17 R. J. Sutton, M. R. Filip, A. A. Haghighirad, N. Sakai, B. Wenger, F. Giustino and H. J. Snaith, Cubic or Orthorhombic? Revealing the Crystal Structure of Metastable Black-Phase $CsPbI_3$ by Theory and Experiment, *ACS Energy Lett.*, 2018, **3**, 1787–1794.

18 F. Ke, C. Wang, C. Jia, N. R. Wolf, J. Yan, S. Niu, T. P. Devereaux, H. I. Karunadasa, W. L. Mao and Y. Lin, Preserving a robust $CsPbI_3$ perovskite phase via pressure-directed octahedral tilt, *Nat. Commun.*, 2021, **12**, 461.

19 A. Marronnier, G. Roma, S. Boyer-Richard, L. Pedesseau, J.-M. Jancu, Y. Bonnassieux, C. Katan, C. C. Stoumpos, M. G. Kanatzidis and J. Even, Anharmonicity and Disorder in the Black Phases of Cesium Lead Iodide Used for Stable Inorganic Perovskite Solar Cells, *ACS Nano*, 2018, **12**, 3477–3486.

20 C. Yi, J. Luo, S. Meloni, A. Boziki, N. Ashari-Astani, C. Grätzel, S. M. Zakeeruddin, U. Röthlisberger and M. Grätzel, Entropic stabilization of mixed A-cation ABX3 metal halide perovskites for high performance perovskite solar cells, *Energy Environ. Sci.*, 2016, **9**, 656–662.

21 P. Marin-Villa, P. Gila-Herranz, M. Jimenez-Ruiz, A. Ivanov, J. Armstrong, K. Druzbicki and F. Fernandez-Alonso, Molecular Derailment *via* Pressurization in Methylammonium Lead Iodide, *ChemRxiv*, 2025, DOI: **10.26434/chemrxiv-2025-jd7bj**.

22 P. S. Whitfield, N. Herron, W. E. Guise, K. Page, Y. Q. Cheng, I. Milas and M. K. Crawford, Structures, Phase Transitions and Tricritical Behavior of the Hybrid Perovskite Methyl Ammonium Lead Iodide, *Sci. Rep.*, 2016, **6**, 42831.

23 O. J. Weber, D. Ghosh, S. Gaines, P. F. Henry, A. B. Walker, M. S. Islam and M. T. Weller, Phase Behavior and Polymorphism of Formamidinium Lead Iodide, *Chem. Mater.*, 2018, **30**, 3768–3778.

24 T. Chen, W.-L. Chen, B. J. Foley, J. Lee, J. P. C. Ruff, J. Y. P. Ko, C. M. Brown, L. W. Harriger, D. Zhang and C. Park, *et al.*, Origin of Long Lifetime of Band-edge Charge Carriers in Organic–inorganic Lead Iodide Perovskites, *Proc. Natl. Acad. Sci. U. S. A.*, 2017, **114**, 7519–7524.

25 S. Kawachi, M. Atsumi, N. Saito, N. Ohashi, Y. Murakami and J. Yamaura, Structural and Thermal Properties in Formamidinium and Cs-Mixed Lead Halides, *J. Phys. Chem. Lett.*, 2019, **10**, 6967–6972.

26 K. Druzbicki, R. Laven, J. Armstrong, L. Malavasi, F. Fernandez-Alonso and M. Karlsson, Cation Dynamics and Structural Stabilization in Formamidinium Lead Iodide Perovskites, *J. Phys. Chem. Lett.*, 2021, **12**, 3503–3508.

27 S. Dutta, E. Fransson, T. Hainer, B. M. Gallant, D. J. Kubicki, P. Erhart and J. Wiktor, Revealing the Low Temperature Phase of $FAPbI_3$ using A Machine-Learned Potential, *J. Am. Chem. Soc.*, 2025, DOI: **10.1021/jacs.5c05265**.

28 D. H. Fabini, T. Hogan, H. A. Evans, C. C. Stoumpos, M. G. Kanatzidis and R. Seshadri, Dielectric and Thermodynamic Signatures of Low-Temperature Glassy Dynamics in the Hybrid Perovskites $CH_3NH_3PbI_3$ and $HC(NH_2)_2$, *J. Phys. Chem. Lett.*, 2016, **7**, 376–381.

29 R. A. Evarestov, E. A. Kotomin, A. Senocrate, R. K. Kremer and J. Maier, Firstprinciples comparative study of perfect and defective $CsPbX_3$ (X = Br, I) crystals, *Phys. Chem. Chem. Phys.*, 2020, **22**, 3914–3920.

30 P. Marín-Villa, A. Arauzo, K. Drużbicki and F. Fernandez-Alonso, Unraveling the Ordered Phase of the Quintessential Hybrid Perovskite $MAPbI_3$Thermophysics to the Rescue, *J. Phys. Chem. Lett.*, 2022, **13**, 8422–8428.

31 M. Moratalla, J. F. Gebbia, M. A. Ramos, L. C. Pardo, S. Mukhopadhyay, S. Rudic, F. Fernandez-Alonso, F. J. Bermejo and J. L. Tamarit, Emergence of Glassy Features in Halomethane Crystals, *Phys. Rev. B*, 2019, **99**, 024301.

32 W. A. Phillips, Tunneling states in amorphous solids, *J. Low Temp. Phys.*, 1972, **7**, 351–360.

33 P. W. Anderson, B. I. Halperin and C. M. Varma, Anomalous low-temperature thermal properties of glasses and spin glasses, *Philos. Mag.*, 1972, **25**, 1–9.

34 D. A. Parshin, Interactions of soft atomic potentials and universality of low-temperature properties of glasses, *Phys. Rev. B*, 1994, **49**, 9400–9418.

35 U. Buchenau, Y. M. Galperin, V. L. Gurevich, D. A. Parshin, M. A. Ramos and H. R. Schober, Interaction of soft modes and sound waves in glasses, *Phys. Rev. B: Condens. Matter Mater. Phys.*, 1992, **46**, 2798–2808.

36 R. A. Kerner, E. D. Christensen, S. P. Harvey, J. Messinger, S. N. Habisreutinger, F. Zhang, G. E. Eperon, L. T. Schelhas, K. Zhu, J. J. Berry and D. T. Moore, Analytical Evaluation of Lead Iodide Precursor Impurities Affecting Halide Perovskite Device Performance, *Appl. Energy Mater.*, 2022, **6**, 295–301.

37 L. D. Whalley, R. Crespo-Otero and A. Walsh, H-Center and V-Center Defects in Hybrid Halide Perovskites, *Energy Lett.*, 2017, **2**, 2713–2714.

38 J. A. Steele, V. Prakasam, H. Huang, E. Solano, D. Chernyshov, J. Hofkens and M. B. J. Roeffaers, Trojans That Flip the Black Phase: Impurity-Driven Stabilization and Spontaneous Strain Suppression in -$CsPbI_3$ Perovskite, *J. Am. Chem. Soc.*, 2021, **143**, 10500–10508.

39 *Amorphous Solids: Low-Temperature Properties*, ed. W. A. Phillips, Springer Berlin Heidelberg, 1981.

40 R. C. Zeller and R. O. Pohl, Thermal Conductivity and Specific Heat of Noncrystalline Solids, *Phys. Rev. B*, 1971, **4**, 2029–2041.

41 P. Debye, *Zur Theorie der spezifischen Wärmen. Ann. Phys.*, 1912, **344**, 789–839.

42 K. Druzbicki, M. Gaboardi and F. Fernandez-Alonso, Dynamics Spectroscopy with Neutrons—Recent Developments Emerging Opportunities, *Polymers*, 2021, **13**, 1440.

43 D. B. Straus, S. Guo and R. J. Cava, Kinetically Stable Single Crystals of Perovskite-Phase $CsPbI_3$, *J. Am. Chem. Soc.*, 2019, **141**, 11435–11439.

44 J. P. Perdew, A. Ruzsinszky, G. I. Csonka, O. A. Vydrov, G. E. Scuseria, L. A. Constantin, X. Zhou and K. Burke, Restoring the Density-Gradient Expansion for Exchange in Solids and Surfaces, *Phys. Rev. Lett.*, 2008, **100**, 136406.

45 K. Druzbicki, P. Gila-Herranz, P. Marin-Villa, M. Gaboardi, J. Armstrong and F. Fernandez-Alonso, Cation Dynamics as Structure Explorer in Hybrid Perovskites The Case of $MAPbI_3$, *Cryst. Growth Des.*, 2023, **24**, 391–404.

46 P. Marin-Villa, M. Gaboardi, B. Joseph, F. Alabarse, J. Armstrong, K. Druzbicki and F. Fernandez-Alonso, Methylammonium Lead Iodide across Physical Space: Phase Boundaries and Structural Collapse, *J. Phys. Chem. Lett.*, 2025, **16**, 184–190.

47 J. Kaczkowski and I. Plowas-Korus, The Vibrational and Thermodynamic Properties of $CsPbI_3$ Polymorphs: An Improved Description Based on the SCAN meta-GGA Functional, *J. Phys. Chem. Lett.*, 2021, **12**, 6613–6621.

48 A. van Hattem, J.-C. Griveau, E. Colineau, A. J. E. Lefering, R. J. M. Konings and A. L. Smith, Low-Temperature Heat Capacity of $CsPbI_3$, Cs_4PbI_6, and $Cs_3Bi_2I_9$, *J. Phys. Chem. C*, 2023, **127**, 22808–22816.

49 M. A. Ramos, Are universal ''anomalous'' properties of glasses at low temperatures truly universal?, *Low Temp. Phys.*, 2020, **46**, 104–110.

50 L. D. Whalley, P. van Gerwen, J. M. Frost, S. Kim, S. N. Hood and A. Walsh, Giant Huang–Rhys Factor for Electron Capture by the Iodine Intersitial in Perovskite Solar Cells, *J. Am. Chem. Soc.*, 2021, **143**, 9123–9128.

51 R. M. Dimeo, Visualization and measurement of quantum rotational dynamics, *Am. J. Phys.*, 2003, **71**, 885–893.

